Electronic Supporting Information

Binding Low Crystalline MoS_2 Nanoflakes on Nitrogen-Doping Carbon Nanotube: Towards High-Rate Lithium and Sodium Storage

Tianjing Wu,[a] *Mingjun Jing,*[a,b]* *Yong Liu,*[a,]* *Xiaobo Ji*[a]

[a]State Key Laboratory of Powder Metallurgy, Central South University, Changsha, 410083, China.

[b]College of Chemistry and Chemical Engineering, Hunan Institute of Science and Technology, Yueyang, 414006, China.

*E-mail: jingmingjun@csu.edu.cn; yonliu@csu.edu.cn

Tel: +86-731-88879616; Fax: +86-731-88879616

Table of Contents

Methods Section

Material Characterizations

The X-ray diffractometer (XRD, Rigaku D/max 2550 VB^{+}) with Cu Kα radiation was utilized to investigate the phase structure of materials at a scanning rate of 5^{o} min^{-1}. Scanning electron microscopy (SEM, JSM-6510LV) was further used to study the morphology of the samples. And the morphology character and atomic arrangement were explored via transmission electron microscopy (TEM, JEM-2100F) and high-resolution transmission electron microscopy (HRTEM, JEM-2100F). The elemental analysis and surface chemical composition of samples were carried out through energy-dispersive X-ray spectroscopy (EDS) and X-ray Photoelectron Spectroscopy (XPS, ESCALab250) with the C1s photoelectron peak at 284.6 eV as the reference. The content analysis of composite was measured via thermogravimetric analysis (TGA, NETZSCH STA449F3) from 30 to 700 ^{o}C with a heating rate of 5 ^{o}C min^{-1} in air. Moreover, the specific surface area of materials was determined using nitrogen adsorption isotherms at 77K with Brunauer-Emmett-Teller (BET, Micromeritics, ASAP 2020). Raman spectrometer (HORIBA Labram HR Evolution) was used to collect raman spectra of as-prepared products.

Electrochemical Measurements

The electrode can be fabricated as follows process. The active material (70 mg) and super P (15 mg) were firstly blended well, and then this mixture was added into the polyvinylidene fluoride (PVDF, 15 mg) binder with N-methyl-2-pyrrolidone (NMP) as solvent under whisking for 12 h. The as-formed homogeneous slurry was coated onto Cu foil and air-dried at 50 ^{o}C. Finally, the working electrodes with the mass loading of 1.0~1.3 mg were obtained after further drying in a vacuum at 80 ^{o}C for 12 h. The electrochemical performances of samples were measured in a CR2016 coin cell, that was assembled in an argon filled glovebox (H_2O < 0.5 ppm, O_2 < 0.5 ppm). For LIBs, Li foil was as both counter electrode and reference electrode. The electrolyte was a solution of 1 M $LiPF_6$ in ethylene carbonate/dimethyl carbonate (volume ratio of 1:1). While, Na foil was as both counter electrode and reference electrode for SIBs. And the electrolyte was a 1 M $NaClO_4$ solution in ethylene carbonate and propylene carbonate system (volume ratio of 1:1). Galvanostatic discharge/charge files of electrodes were performed on Land CT2001A battery cycler at various current densities. Cyclic voltammetry (CV) curves at various scanning rates and Electrochemical impedance measurements (EIS) at the open–circuit voltages were further investigated on MULTI AUTOLAB M204 (MAC90086).

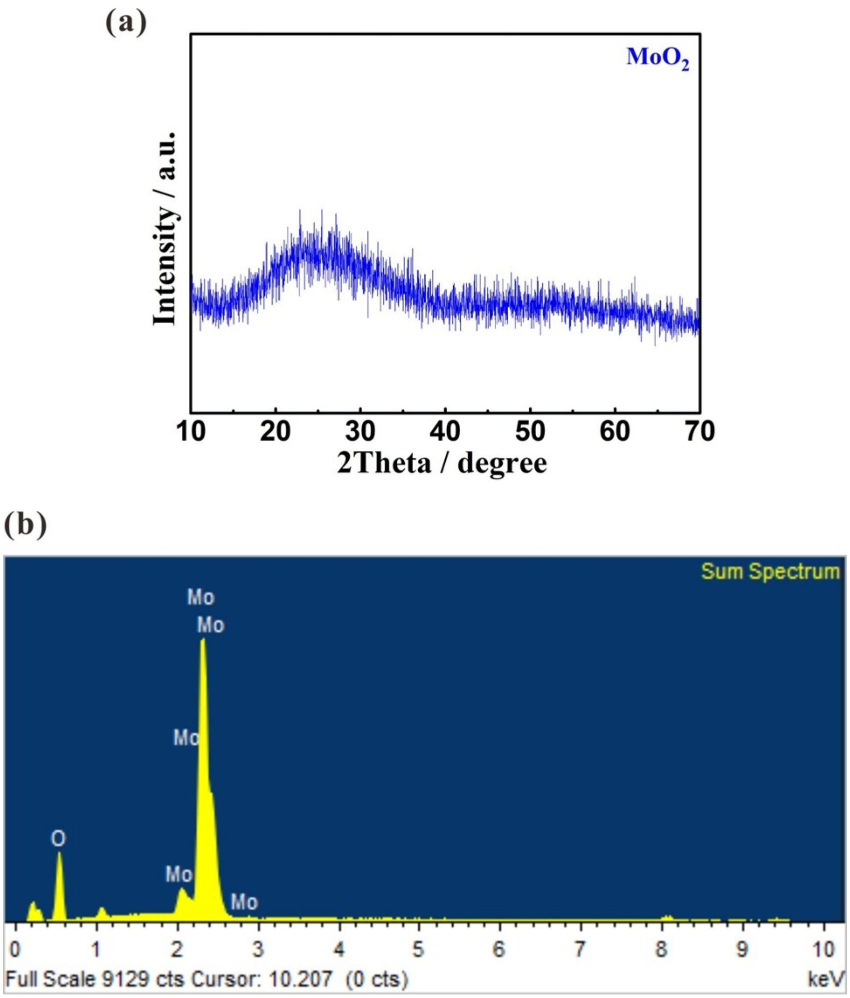

Fig. S1. (a) XRD pattern and (b) EDS of the product after alternating current treatment.

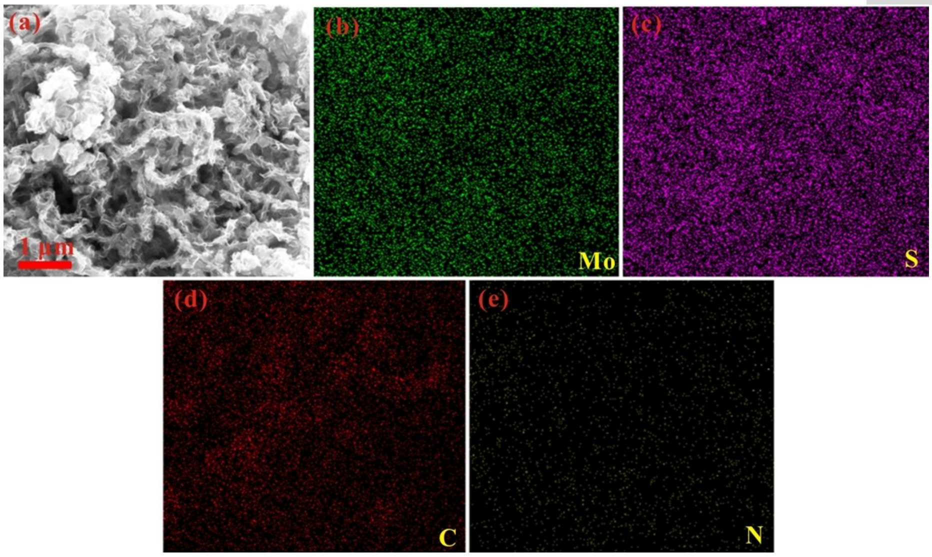

Fig. S2. The SEM (a) and elemental mapping images (b-e) of MoS_2/N-CNT.

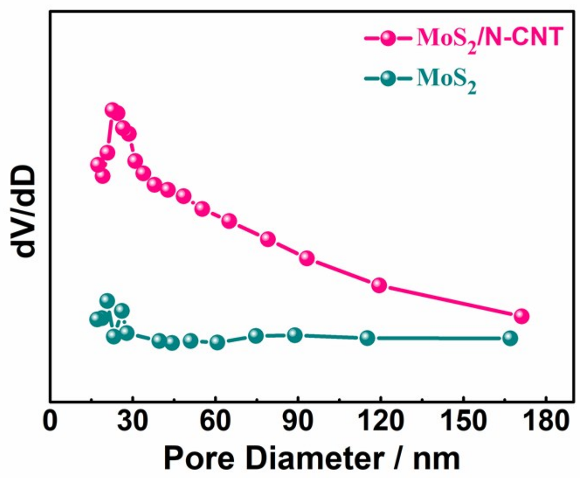

Fig. S3. The pore size distribution results of MoS_2 and MoS_2/N-CNT based on their adsorption curves.

Moreover, the pore size distribution results of MoS_2 and MoS_2/N-CNT have been further analyzed by the Barrett-Joyner-Halenda method, as is shown in Fig. S3. The MoS_2/N-CNT composite exhibits some mesopores and macropores originating from the introduction of CNT, which is beneficial to ion transport.

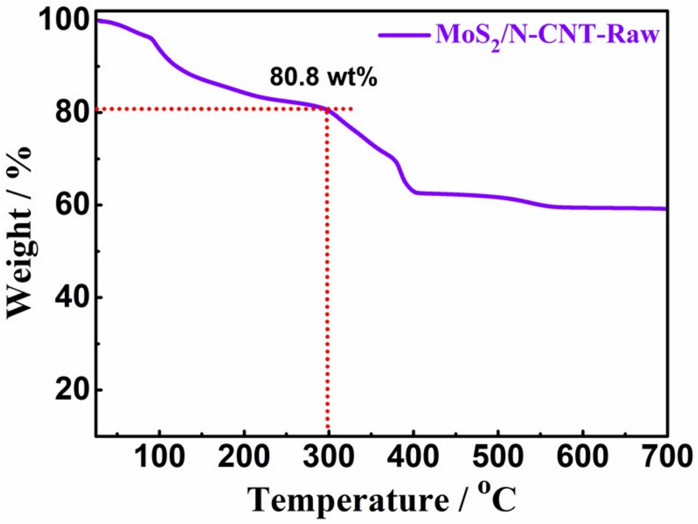

Fig. S4. TG curve of MoS_2/N-CNT-Raw composite from room temperature to 700 ^{o}C under air.

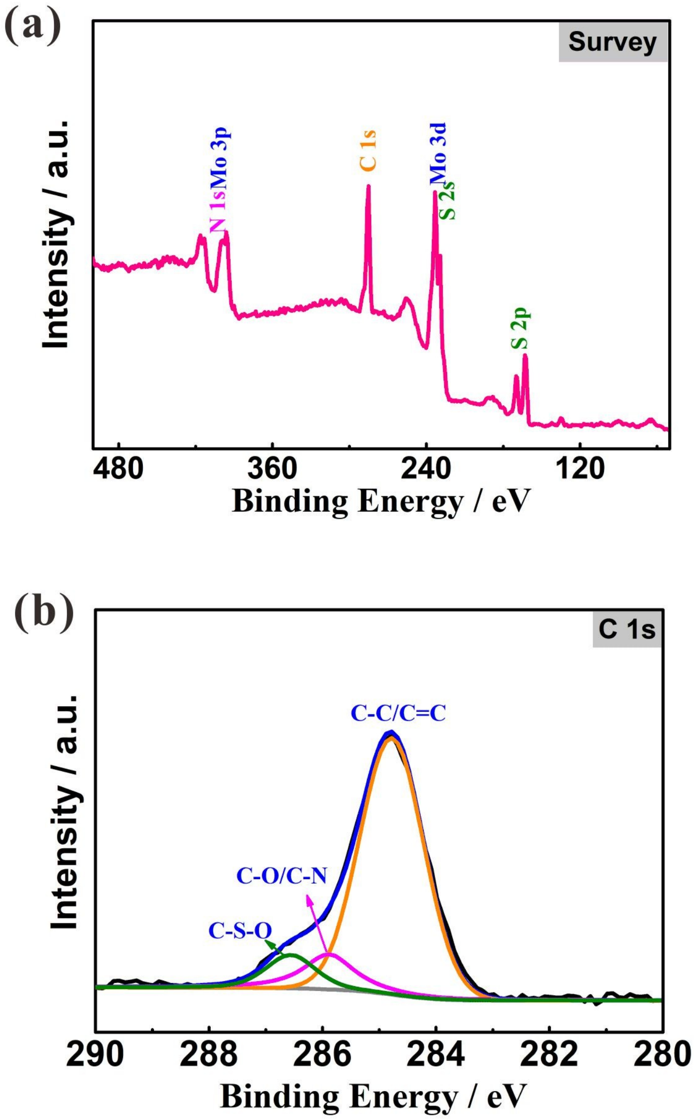

Fig. S5. (a) The survey spectrum of MoS_2/N-CNT composite. (b) C 1s XPS spectrum of MoS_2/N-CNT composite.

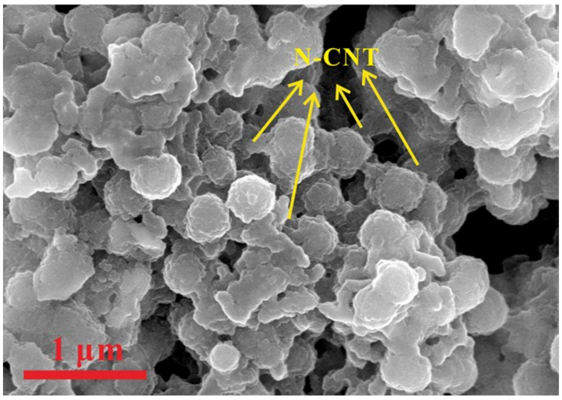

Fig. S6. SEM of MoS_2/N-CNT electrode after 800 cycles at a current density of 2 A g^{-1} for LIBs.

The SEM result of MoS_2/N-CNT electrode has been measured after 800 cycles at a current density of 2 A g^{-1} for LIBs, which is shown in Fig. S6. It can be seen that MoS_2 displays volume expansion. While the N-CNT can still well anchor the MoS_2 as an integrated electrode after cycles. Herein, the introduction of N-CNT can be helpful to maintain the stable structure and improve the cycling stability.

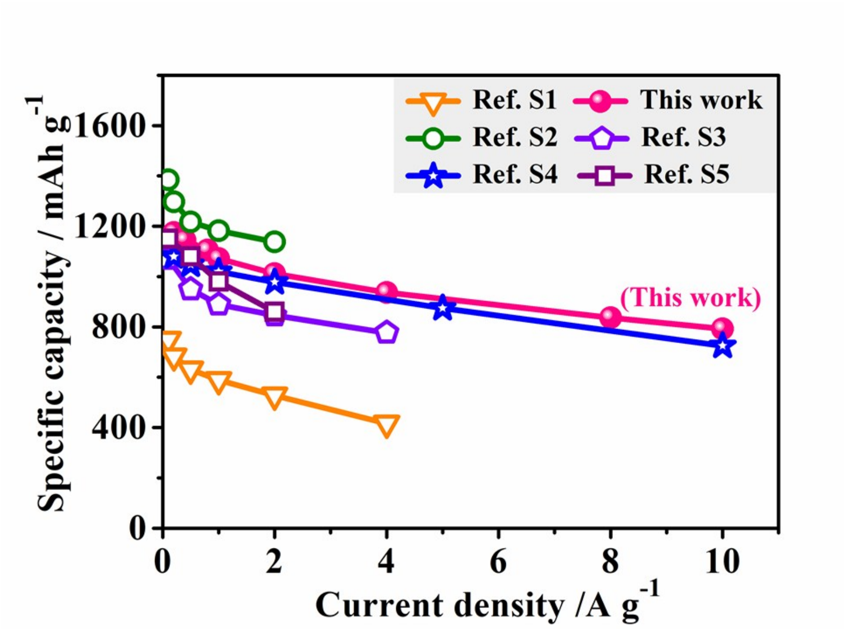

Fig. S7. Rate behavior of MoS_2-based anodes for LIBs from previous literatures compared against the current work.

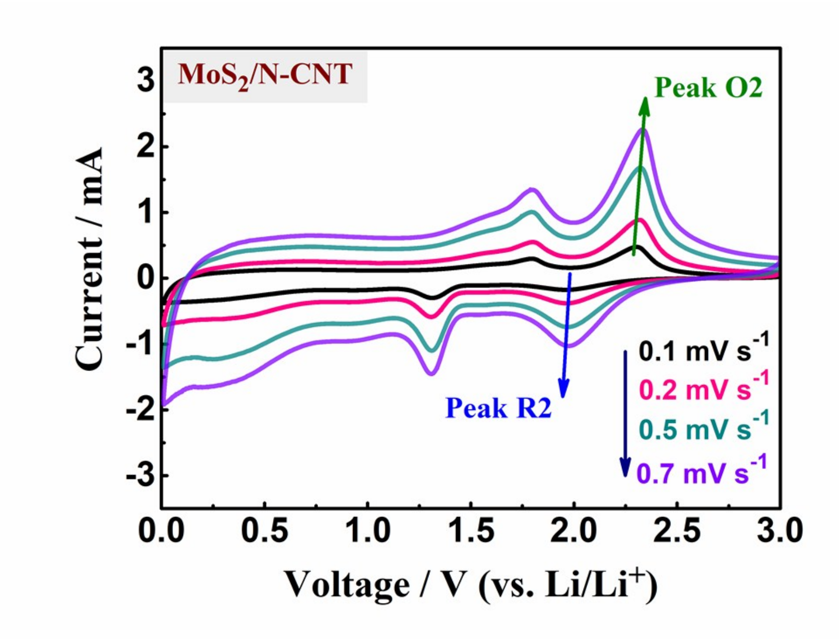

Fig. S8. CV curves of MoS_2/N-CNT electrode at various scan rates from 0.1 mV s^{-1} to 0.7 mV s^{-1}.

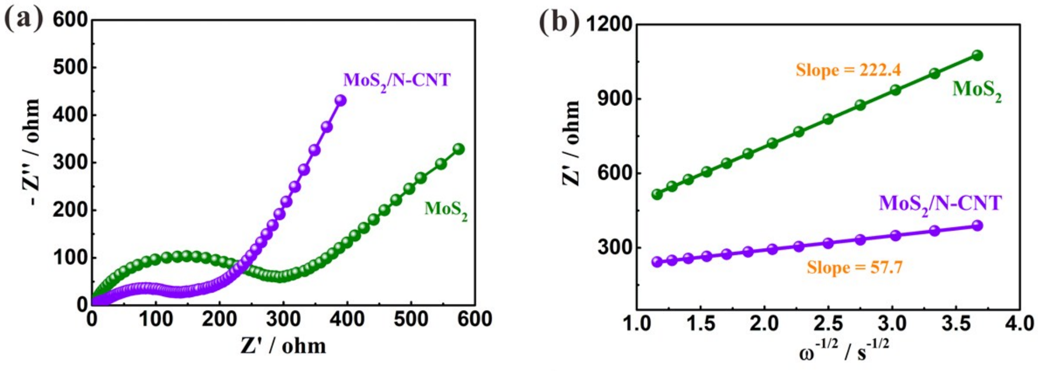

Fig. S9. (a) Nyquist plots of pure MoS_2 and MoS_2/N-CNT composite after 100 cycles at 200 mA g^{-1} for SIBs. (b) Z' vs $w^{-1/2}$ plots of MoS_2 and MoS_2/N-CNT for Warburg impedance analysis.

The EIS analysis of pure MoS_2 and MoS_2/N-CNT composite for SIBs has been added in Fig. S9. The Nyquist plots of pure MoS_2 and MoS_2/N-CNT composite are abtained after 100 cycles at 200 mA g^{-1} in Fig. S9a. It shows the resistance R_{ct} of MoS_2/N-CNT is obvious smaller than pure MoS_2 electrode. Also, the Warburg impedance coefficient (σ) relative to Z' have been further calculated, as is shown in Fig. S9b. The slop of MoS_2/N-CNT (57.7) is much smaller than that of MoS_2 (222.4), illustrating the higher Na^+ diffusion rate of this composite electrode.

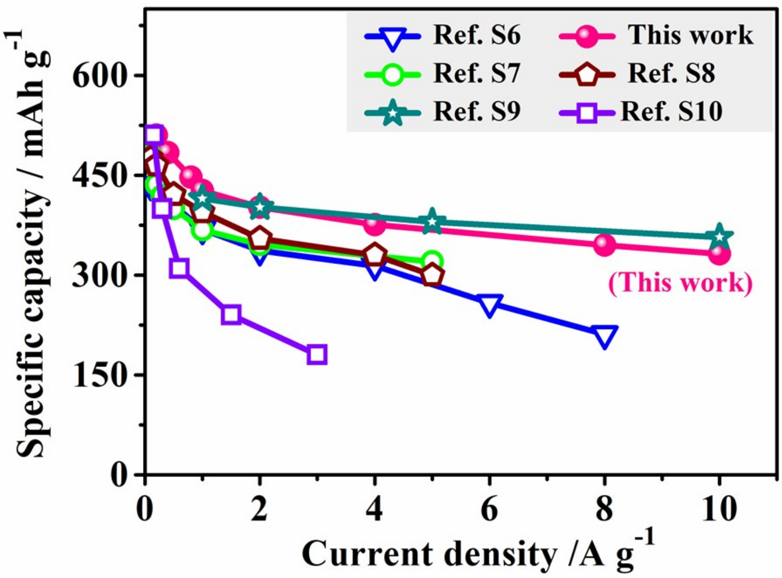

Fig. S10. Rate behavior of MoS_2-based anodes for SIBs from previous literatures compared against the current work.

Table S1 The electrical conductivity data of pure MoS_2 and MoS_2/N-CNT.

Sample	Electrical Conductivity (S cm^{-1})
MoS_2	8.21×10^{-5}
MoS_2/N-CNT	78.12

The electrical conductivity of pure MoS_2 and MoS_2/N-CNT has been investigated by four-point probe tester (SDY-40, Guangdong, China). The data has been presented in Table S1 based on the average values of three samples for each electrode. The MoS_2/N-CNT shows significantly higher electrical conductivity than that of pure MoS_2.

References

S1 B. Chen, Y. Meng, F. He, E. Liu, C. Shi, C. He, L. Ma, Q. Li, J. Li, N. Zhao, *Nano Energy* **2017**, *41*, 154.

S2 G. Wang, J. Zhang, S. Yang, F. Wang, X. Zhuang, K. Müllen, X. Feng, *Adv. Energy Mater.* **2018**, *8*, 1702254.

S3 L. Ma, B. Zhao, X. Wang, J. Yang, X. Zhang, Y. Zhou, J. Chen, *ACS Appl. Mater. Interfaces* **2018**, *10*, 22067.

S4 Y. Jiao, A. Mukhopadhyay, Y. Ma, L. Yang, A. M. Hafez, H. Zhu, *Adv. Energy Mater.* **2018**, *8*, 1702779.

S5 L. Jiang, B. Lin, X. Li, X. Song, H. Xia, L. Li, H. Zeng, *ACS Appl. Mater. Interfaces* **2016**, *8*, 2680.

S6 R. Wang, S. Gao, K. Wang, M. Zhou, S. Cheng, K. Jiang, *Sci. Rep.* **2017**, *7*, 7963.

S7 Y. Teng, H. Zhao, Z. Zhang, L. Zhao, Y. Zhang, Z. Li, Q. Xia, Z. Du, K. Świerczek, *Carbon* **2017**, *119*, 91.

S8 J. Wu, Z. Lu, K. Li, J. Cui, S. Yao, M. Ihsan-ul Haq, B. Li, Q.-H. Yang, F. Kang, F. Ciucci, J.-K. Kim, *J. Mater. Chem. A* **2018**, *6*, 5668.

S9 B. Chen, H. Lu, J. Zhou, C. Ye, C. Shi, N. Zhao, S. Z. Qiao, *Adv. Energy Mater.* **2018**, 1702909.

S10 D. Xie, X. Xia, Y. Wang, D. Wang, Y. Zhong, W. Tang, X. Wang, J. Tu, *Chem. Eur. J.* 2016, *22*, 11617.